Measurement of CO pressures in the ultrahigh vacuum regime using resonance-enhanced multiphoton-ionization time-of-flight mass spectroscopy

J. Patrick Looney
Thermophysics Division, National Institute of Standards and Technology, Gaithersburg, Maryland 20899

Joel E. Harrington[a] and Kermit C. Smyth
Fire Science Division, National Institute of Standards and Technology, Gaithersburg, Maryland 20899

Thomas R. O'Brian[a] and Thomas B. Lucatorto
Electron and Optical Physics Division, National Institute of Standards and Technology, Gaithersburg, Maryland 20899

(Received 22 April 1993; accepted 21 August 1993)

An evaluation is made of measurements of CO pressures in the UHV regime using resonance-enhanced multiphoton ionization coupled with time-of-flight mass spectroscopy (REMPI-TOFMS). It has been found that once the REMPI-TOFMS system has been calibrated, quantitative measurement of CO pressures as low as 10^{-10} Pa is possible, even in overwhelming N_2 backgrounds. With compensation for laser pulse energy variations, we find measurements with uncertainties of 10%–15% are possible for pressures down to 10^{-7} Pa, and an ultimate detection limit for CO pressures of 10^{-10} Pa for our measurement system. In this study, the REMPI-TOFMS system was calibrated using a pressure division technique along with a spinning rotor gage. The ionization of CO is achieved using 230 nm radiation to excite the $B\,^1\Sigma^+$ state of CO at 10.8 eV via a two-photon absorption and then ionizing some of the excited state molecules by the absorption of an additional photon from the laser beam.

I. INTRODUCTION

Quantitative measurement of total and partial pressures in the UHV regime for noninert gases such as H_2O, O_2, CO, and CO_2 is one of many long-standing problems in vacuum technology. One of the difficulties which arises in making measurements of the pressure of these gases using commonly available vacuum instrumentation, e.g., ionization gages or mass spectrometers equipped with hot cathode electron impact ionizers, is that the presence of hot filaments usually results in some perturbation of the vacuum environment and interferes with the measurement process. One example is the interaction of oxygen with a hot tungsten filament, such as in a common Bayard–Alpert (BA) type ionization gage, which results in the generation of several percent each of CO and CO_2 from carbon impurities present in the filament material.[1,2] Another example is the large, systematic error in oxygen pressure determination that arises at low pressures ($<10^{-4}$ Pa) due to large "false" currents generated within the gage from electron stimulated desorption of atomic oxygen from the gage grid structure.[3] To better understand and diagnose these and other problems, independent techniques for measuring and monitoring low pressures of "active" gases are highly desirable.

To this end we have undertaken an investigation of the use of species specific laser-based ionization along with *time-of-flight mass spectroscopic* (TOF-MS)-based ion detection for the quantitative measurement of CO pressures in the UHV regime. Laser ionization has the attractive feature that it is less intrusive than hot filament electron impact ionization and is potentially applicable to the measurement of low densities of active or noninert gases. Further, there have been a number of studies reported which demonstrate the fundamental sensitivity of laser ionization-based techniques for measuring gas densities at low pressure. Zacharias *et al.*,[4] Chein and Sogard,[5] and Kokobun *et al.*,[6] for example, all have reported low pressure gas species detection ("ultrasensitive detection") using laser ionization techniques, but have not quantified their measurement uncertainties. However, the promise of any new measurement technique can only be assessed after critical evaluation of its precision, reproducibility and sensitivity. This study represents the first attempt to elucidate and quantify these attributes for laser ionization based measurement of pressures in the UHV regime.

For some time laser-based multiphoton ionization (MPI) has been used to detect low concentrations of atoms, molecules, and radical intermediates in a wide variety of applications including analytical chemistry (isotopic analysis)[7–9] and chemical flame diagnostics.[10–12] These applications all use a resonance-enhanced MPI (REMPI) approach whereby the specific atom or molecule under study is ionized by absorbing one or more photons to an excited electronic state and then absorbing one or more additional photons from the laser beam to promote an electron to an energy above the ionization threshold. The critical advantage is that by judicious choice of the electronic transitions used for the ionization process, REMPI of gas phase molecules provides excellent species specificity in ion production via wavelength tuning. When coupled with mass spectroscopic ion filtering and detection, one can obtain highly selective species identification even in the pres-

[a]NIST/NRC Postdoctoral Fellow.

ence of interferences from species of the same unit mass. Furthermore, REMPI can also provide state resolved information to aid in the diagnostics of physical and chemical processes.

Studies by Zacharias and co-workers[4] using REMPI with quadrupole mass spectroscopic based ion detection have demonstrated that detection of NO is feasible for partial pressures as low as 10^{-10} Pa with excellent isotopic selectivity. In a more recent paper, Rottke and Zacharias[13] demonstrated state-resolved CO detection in the range of 10^{-9} Pa in a single rotational level. In this latter study vacuum ultraviolet radiation at 115 nm was employed to directly excite the $B\,^1\Sigma^+$ state of CO at 10.8 eV and a second photon at 345 nm then ionized some of the electronically excited molecules. The CO^+ ions were detected using a TOF-MS equipped with a secondary electron multiplier. As it was apparently not possible for Rottke and Zacharias[13] to generate test pressures much below 10^{-4} Pa directly, the potential for high sensitivity CO detection using this scheme was demonstrated by measurements performed on very high rotational levels that are only weakly populated at room temperature (i.e., have low partial pressure). Curiously, Rottke and Zacharias[13] deemed the CO detection sensitivity using two-photon excitation of the $B\,^1\Sigma^+$ state with 230 nm radiation as low, and incorrectly quote a detection limit of only 10 Pa using this scheme. In this paper we will demonstrate a detection sensitivity near 10^{-10} Pa using the two-photon excitation of the $B\,^1\Sigma^+$ state with 230 nm radiation, a detection sensitivity which is similar to that demonstrated by Rottke and Zacharias with single-photon excitation of the $B\,^1\Sigma^+$ state.

Although there have been a number of studies which demonstrate the fundamental sensitivity of REMPI based measurements, only a small subset of these address the issues associated with quantitative measurement of gas densities. The most thorough discussion of the issues involved is that by Cool,[14] who described in detail the approach to quantitative measurement of NO densities. Cool clearly points out the need to characterize and monitor laser parameters so that reproducible measurements are obtainable and to the utility of developing models for the measured ion signals to elucidate the influence of the major parameters affecting density measurements. We develop a similar model, applicable to our experimental situation, in Sec. IV.

Chein and Sogard[5] and Kokobun *et al.*[6] have recently reported on low pressure gas species detection using nonresonant laser ionization. In nonresonant ionization, ions are produced by using a laser of intensity sufficiently high as to induce the simultaneous absorption of multiple photons which promotes an electron directly into the ionization continuum. For lasers of sufficiently high intensity, non-resonant ionization is essentially nondiscriminating and theoretically capable of ionizing all species present within the laser beam's focal volume. Nonresonant ionization might then be attractive for residual gas determination where entire mass spectra are desired. Even though the cross sections for nonresonant ionization are typically much smaller than the effective cross sections for REMPI, nonresonant ionization can be accomplished with fixed frequency lasers which have peak intensities that are much larger than tunable systems in the same wavelength range and so ion yields per pulse can be comparable. One advantage is that only one laser is needed; typically a pulsed excimer or the second or third harmonic output from a Nd:YAG laser can be utilized for the ionizing radiation. This can greatly reduce cost and complexity compared to the tunable laser systems required for REMPI.

There are many potential disadvantages in using nonresonant radiation for the ionization of small molecules. For example, nonresonant ionization cross sections vary greatly from species to species. Further, nonresonant ionization will not help to distinguish between molecules with the same molecular weight (e.g., CO and N_2). Thus, even though nonresonant ionization can yield entire mass spectra, the calibration and interpretation can be quite a complex task. Another disadvantage is that nonresonant ionization schemes typically employ much larger laser fluences and can create large background pressures due to photon stimulated desorption from surfaces within the vacuum chamber. These and more subtle problems could, perhaps, limit the usefulness of nonresonant ionization for pressure measurements in the UHV regime.

In this investigation we demonstrate that reproducible measurements of CO pressure are possible using REMPI coupled with a TOF-MS for the ion filtering and detection. The TOF-MS system used here has a dynamic range of about 10^6 in the ion signal, thereby allowing for the quantitative measurement of gas densities over a wide range in total and partial pressures. The results of these experiments demonstrate that CO pressures as low as 10^{-7} Pa can be measured with an uncertainty of about 10%–15%, and pressures down to 10^{-9} Pa can be measured with an uncertainty of 20%–30%. Under the present experimental conditions, the ultimate CO detection limit is estimated to be about 10^{-10} Pa. We also address some of the problems associated with the development of a quantitative low density measurement capability in the UHV regime using REMPI.

II. EXPERIMENTAL APPROACH

One of the first considerations involved when using REMPI for the generation of ions is the identification of favorable features in the ionization spectrum of a molecule which can be used for quantitative measurements. To some extent the "favorable" characteristics of an ionization feature depend upon the measurement application. In the present set of experiments we are mainly interested in determining the number density of CO molecules in a high vacuum environment with the highest possible sensitivity. In this study we have chosen to use a two-photon resonant, three-photon ionization scheme which proceeds through the $B\,^1\Sigma^+(v'=0)$ state at 10.78 eV. A diagram of this photoionization process is given in Fig. 1. The excitation of CO through the $B\,^1\Sigma^+ \leftarrow X\,^1\Sigma^+$ (0,0) two-photon absorption at 230 nm using linearly polarized light results in a strong, compact Q-branch head which exhibits little rotational structure.[15] Further, the $B\,^1\Sigma^+(v'=0)$ state exhib-

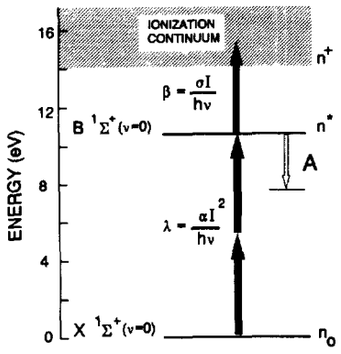

FIG. 1. A schematic energy level diagram for the CO molecule showing the photoionization scheme employed in this study and the parameters used in the rate equation model of Sec. IV. Here λ, β, and A are the two-photon absorption, ionization, and radiative decay rates, respectively.

its negligible predissociation at low J',[13,16] has a moderately long radiative lifetime ($\approx$25 ns),[17] and has a large cross section for photoionization by an additional 230 nm photon ($\sigma \geqslant 10^{-17}$ cm^2).[18] For the moderate laser intensities ($\approx 10^9$ W/cm^2) attainable with our laser system, the ionization process will dominate the loss mechanisms from the $B\,^1\Sigma^+(v'=0)$ state, and a strong ionization signal results. As N_2 exhibits no resonant ionization spectrum at 230 nm and has a negligible nonresonant signal for the laser intensities used in this study, there is no potential for contribution from unwanted N_2 ion signals at $m/e=28$ in the TOF-MS traces. Thus, this ionization scheme is, in many ways, ideal for quantitative measurements of low CO pressures.

A. Laser system

A schematic diagram of the optical system used in the present study is given in Fig. 2. To generate the requisite 230 nm radiation, the output of the third harmonic of a pulsed Nd:YAG laser at 355 nm (70 mJ/pulse, 10 ns duration, 10 Hz) was used to pump a dye laser with transversely pumped oscillator/preamplifier cells containing

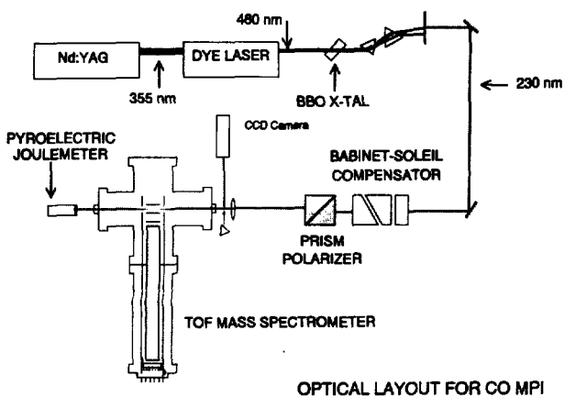

FIG. 2. Schematic diagram of the optical system used in this study.

Coumarin 460 dye. The amplifier output at 460 nm ($\approx$10 mJ/pulse, $\approx$4 ns duration) was then passed through a beta-barium borate (BBO) crystal mounted in an integral microprocessor controlled crystal tracker to produce tunable, linearly polarized radiation near 230 nm with a bandwidth of <0.1 cm^{-1} and pulse energies of $\approx$0.5 mJ/pulse. The laser frequency stability is quoted by the manufacturer to be <0.03 cm^{-1} per 1 °C change in the room temperature ambient. The UV and visible light were separated using a pair of quartz prisms. The UV light was then passed through a UV-grade quartz Babinet–Soleil compensator and then through a prism polarizer/analyzer. By varying the retardance of the laser beam with the Babinet-Soleil compensator, continuously variable attenuation of the laser beam was achieved.

The beam was then focused into the ion collection region of a TOF mass spectrometer (see Sec. II B below) with a 25 cm focal length UV-grade quartz lens. The transmitted UV beam pulse energy was measured with a pyroelectric joulemeter placed just outside the exit window. The pyroelectric joulemeter was calibrated *in situ* against a volume absorbing energy meter located just in front of the 25 cm focusing lens. By placing a 90° turning prism between the focusing lens and the vacuum chamber window, the x–y spatial variation of the laser intensity at the laser focus was measured in room air with a charge-coupled device (CCD) camera having 13.5×11.5 μm pixel dimensions. At its focal point, the laser beam was found to be approximately 200×80 μm, somewhat elliptically shaped with two "hot" spots evident. The spatial profile of the laser beam was clearly not a Gaussian profile, but did not vary appreciably in cross section over the 3 mm collection dimension along its propagation direction. Even with a beam profile which was less than ideal, we found that quantitative measurements were still possible, and by using CCD camera images of the laser intensity profile, we could calculate the dependence of the ion signal on laser pulse energy (laser intensity) with acceptable results.

B. The time-of-flight mass spectrometer

The TOF-MS used in this study is schematically detailed in Fig. 3(a). It consists of a repeller plate and first acceleration grid separated by 19 mm, a 1×3 mm aperture separated by another 15 mm, another acceleration grid, and a 38 cm long grounded drift tube. The ion detector [dual micro channel plate (MCP)] is mounted in a 0.05 mm thick grounded copper cup, which shields the detector and helps focus the ions. The whole TOF-MS was constructed on four 6.35 mm (0.25 in.) 304 stainless steel rods and mounted on a 152 mm (6 in.) conflat-type flange with BNC and MHV electrical feedthroughs. Under normal operating conditions, the repeller was maintained at +500 V and the first grid at +100 V, while the aperture and second acceleration grid were grounded. The MCP ion detector was maintained at −2000 V on the front plate and −200 V on the rear plate with a resulting charging current of 17.5 μA and an overall

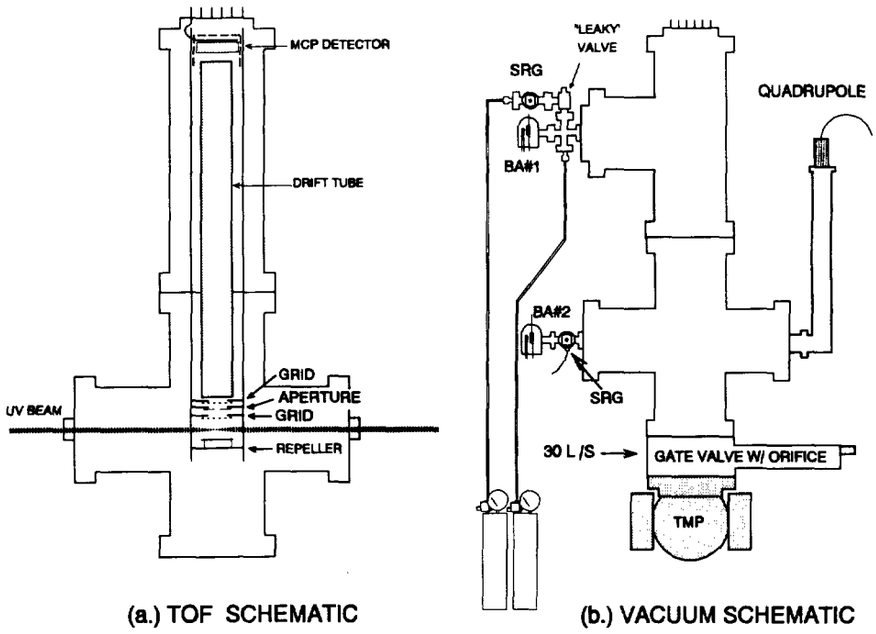

FIG. 3. Schematic diagram of the (a) time-of-flight mass spectrometer system and (b) vacuum system used in this study.

gain of about 10^6. The output from the detector was monitored with a digital storage oscilloscope with 300 MHz bandwidth and 100 Msamples digitization rate.

The aperture limits the spatial region from which ions are collected to be ± 1.5 mm about the center axis of the TOF-MS. Ion trajectory modeling, using SIMION,[19] indicates that the aperture has the added effect of acting as a velocity selector and can affect the collection efficiency depending on the initial ion velocity. The collection efficiency is found to be near unity (>0.99) for those ions which have initial kinetic energies of about 0.2 eV or less. For higher energies, only those ions whose initial velocity is directed at small angles to, or directly along the TOF axis are transmitted to the detector. This limits the temporal width of the arriving ion pulse to ≈ 0.2–0.3 μs for ions with $m/e=28$ and initial kinetic energies less than 2 eV (all of the CO^+ ions in this experiment should have kinetic energies much less than 0.01 eV). The calculated time-of-flight for an ion pulse created 1 mm above the repeller plate is 10.5 μs, in good agreement with the measured time-of-flight of 10.8 μs under similar operating conditions. It was found experimentally that the highest collection efficiencies were obtained with the laser beam focused slightly above the repeller plate. This empirical observation was also confirmed by the ion trajectory modeling.

C. The vacuum system and gaging

The vacuum system [see Fig. 3(b)] is constructed from a 25.4 cm (10 in.) conflat-type six-way cross and tee and pumped with a 500 ℓ/s turbomolecular pump. The vacuum system was baked to 200 °C, and after bakeout the base pressure, as indicated by the hot cathode ionization gages, was in the 10^{-8} Pa range. The main chamber and pump are separated by a 25.4 cm (10 in.) pneumatic gate valve with a 2 cm diam hole drilled in the gate. With the gate valve in the closed position, the effective pumping speed to the chamber due to the hole in the valve is approximately 30–40 ℓ/s. The chamber had two separate gas handling systems composed of ballast tank with leak valve for independent control and delivery of two gas species.

The vacuum chamber was equipped with two glass tubulated Bayard–Alpert (BA) hot cathode ionization gages and a 100 amu quadrupole mass spectrometer, all having tungsten filaments and operating at 1 mA emission current. Collector currents from the BA gages were measured with a picoammeter. The chamber was also equipped with two spinning rotor gages[20,21] (SRGs) which were used for both ionization gage calibration and direct pressure determination. One of the SRGs was mounted directly on the main chamber, the other was mounted on one of the gas inlet lines, directly behind a copper-seated valve which had a small hole drilled into the seat. In the closed position this "leaky" valve had a measured pressure ratio across the valve of 923:1 for CO and N_2. A SRG can only measure, directly, pressures down to $\approx 10^{-4}$ Pa with tolerable uncertainties (1%–5%). By using a SRG/orifice combination (i.e., a pressure divider system) the effective measurement range of the SRG can be extended down to 10^{-7} Pa with uncertainties of 5%–15%.[22]

D. Experimental procedure

The time-of-flight mass spectra and the pulsed output from the pyroelectric joulemeter were recorded with the digital oscilloscope triggered by the output from a fast photodiode placed inside the dye laser housing. Peak heights of the $m/e=28$ ion signal and the pulse height from the py-

roelectric joulemeter for accumulated 500 laser shot averages were recorded along with the output currents from the BA gages and the quadrupole mass spectrometer $m/e=28$ signal. A gated integrator (boxcar), along with a digitizer and computer interface, were used for recording wavelength scans of the MPI spectra.

Ultrahigh purity (>99.99%) CO was introduced into the chamber through one of the ballast tank and leak valve combinations. CO ionization signals were measured as a function of pulse energy and pressure for pulse energies between 0.01 and 0.4 mJ and CO pressures between 10^{-7} and 10^{-4} Pa. The measurements were made at a fixed wavelength at the peak of the CO ionization signal (see Fig. 5, Sec. III A). Most of the data were accumulated by starting at low pressures and working toward higher pressures, but this was not always the case and the direction (pressure increasing or decreasing) did not have any discernable effect on the measurements. Several minutes (5–20) were allowed to pass to reach a new equilibrium after a change in pressure. An established pressure would remain constant (to within a few percent) over the course of several hours, ample time for the completion of the laser measurements. Once the stability of the CO pressure was assured, the dependence of the CO ionization signal on pulse energy was measured. A minimum of three data points (500 laser shot averages) were taken at each pulse energy level. Signals were recorded for pulse energy decreasing and increasing with no observed hysteresis.

Care was taken not to disturb the alignment of the laser system during the course of the measurements as small alignment changes in the dye laser were found to result in concomitant changes in the CO^+ signal levels as large as a factor of 2, presumably due to pointing changes in the output laser beam. The pulse energy of the pump laser was checked frequently as the doubling and tripling KDP crystals in the Nd:YAG needed to be frequently realigned. The laser dye was changed daily to avoid loss of laser pulse energy due to photochemical degradation. It was found that, with care, CO signal levels for a given pressure/pulse energy combination were repeatable to 10%–15% over the course of several (5–7) days.

III. RESULTS

A. The time-of-flight mass spectrum and the resonant MPI spectrum

A low pressure ($\approx 1\times10^{-6}$ Pa) time-of-flight mass spectrum recorded from the digital oscilloscope is shown in Fig. 4. Evident in this trace are two main features, one is the time $t=0$ pulse which is due to scattered UV radiation and the other feature at $t=10.8$ μs is the resonant CO^+ ion signal. Not evident at this gain are the much smaller C^+ and O^+ signals, presumably photodissociation products, which were about 400 and 700 times weaker, respectively.

A very low pressure (6.6×10^{-7} Pa) laser scan for linearly polarized light and wavelengths near 230 nm is shown in Fig. 5 with a numerically simulated spectrum below. This trace, recorded with an estimated laser intensity of 8×10^{8} W/cm^2, shows the very compact nature of

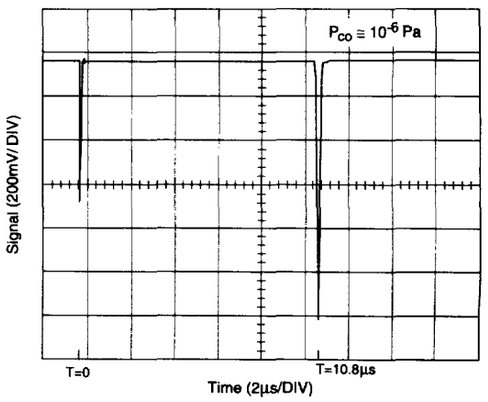

FIG. 4. Time-of-flight mass spectrum recorded at $\approx 1\times10^{-6}$ Pa (7.5×10^{-9} Torr). The peak at $T=0$ is due to scattered UV radiation, and the peak at $T=10.8$ μs is the CO^+ ion signal.

the $B\,^1\Sigma^+ \leftarrow X\,^1\Sigma^+$ (0,0) Q head. No evidence of S or O branch excitation was found. The numerical simulation was calculated using an assumed temperature of 300 K, a Franck–Condon factor of unity and an effective single photon bandwidth of 0.3 cm^{-1} full-width half-maximum. This effective bandwidth includes contributions from lifetime broadening due to ionization and radiative decay, Doppler broadening (≈ 0.1 cm^{-1}) and bandwidth of the dye laser (<0.1 cm^{-1}).

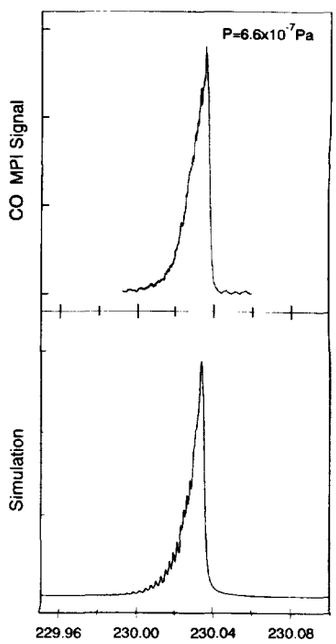

FIG. 5. The CO multiphoton ionization spectrum at 230 nm using linearly polarized light recorded at 6.6×10^{-7} Pa ($=5.0\times10^{-9}$ Torr) (upper trace) and a simulation of the two-photon absorption spectrum of CO near 230 nm (lower trace).

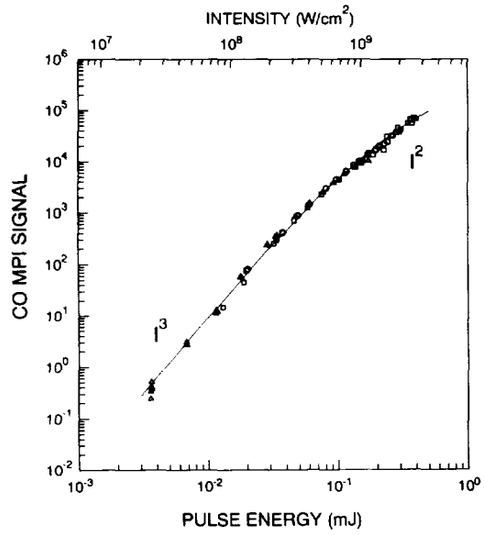

FIG. 6. A log–log plot of the CO REMPI signal as a function of laser intensity. The experimental data are indicated by the discrete symbols (triangles, circles and squares). The theoretical intensity dependence is indicated by the solid line (see Sec. IV).

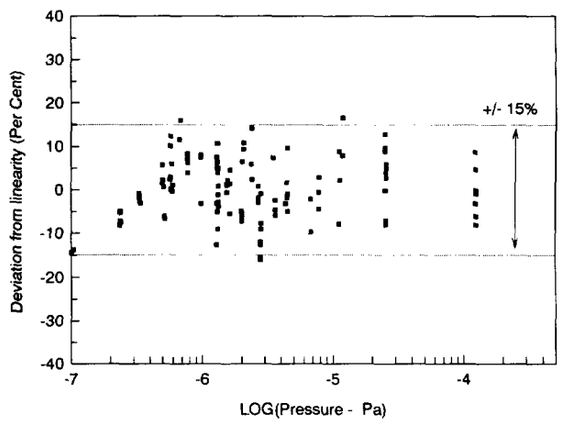

FIG. 7. The deviations from the best-fit linear regression to the corrected CO REMPI signal vs CO pressure. The CO REMPI signals were corrected for changes in the laser pulse energy using the semiempirical model developed in Sec. IV.

B. Intensity dependence

As laser photoionization yields are dependent upon the laser intensity in a nonlinear way, determination of the dependence of the ion signal on laser intensity allows for correction of ionization signals for changes in laser intensity during the course of the measurements. Measurements of the CO REMPI signal versus laser pulse energy were made for a range of CO pressures between 10^{-6} and 10^{-4} Pa over the course of several days. The results of these measurements, scaled for changes in the number density of CO molecules, are displayed in Fig. 6 where each data point plotted represents the average of three individual 500-laser shot averages. For pressures near 10^{-4} Pa and pulse energies above 0.25 mJ/pulse, saturation of the MCP ion detector was observed, and these points were omitted from the figure. Except for MCP detector saturation, there were no systematic differences in the CO REMPI signal versus laser pulse energy curves recorded at the different pressures or on different days. At low laser intensities the observed CO REMPI signal exhibits an I^3 dependence, and at the highest intensities an I^2 dependence. This nonlinear dependence of the ion signal on laser pulse energy (intensity) underscores the need for laser pulse energy (intensity) measurements to correct REMPI signals for laser energy variations.

From Fig. 6 we can see that quantitative measurement of gas densities using REMPI is complicated by the highly nonlinear nature of the ionization process. When n photons are absorbed in the resonant excitation step ($n=2$ in this case) and ionization occurs with the absorption of an additional photon ($n+1$ total photons), ion signals depend upon the laser intensity to the $n+1$ power at low laser intensities. Low laser intensities in these experiments refers to a situation where the rate of ionization is smaller than the total rate of decay out of the intermediate state from other processes. In general, the order of the nonlinearity can be reduced to n as the laser intensity is made large enough that the rate of ionization will be larger than all other loss rates, which include radiative decay, stimulated emission, predissociation and collisional quenching. Further reduction of the order of the nonlinearity of the ionization processes ($<n$) in these experiments from initial state population depletion (i.e., saturation of the two-photon transition) and/or complete ionization in a portion of the focal volume[23] is unlikely for the moderate peak laser intensities ($\approx 10^9$ W/cm^2) available. As discussed in Sec. IV below, the fundamental relationship between the ion yield, gas density and laser parameters is further complicated by considerations of the temporal and spatial characteristics of the excitation laser.

C. REMPI signal dependence on CO pressures

A series of measurements was conducted to determine the precise relationship between the CO pressure and the measured ionization signals. These data were acquired over the course of many days and were taken over a range in CO pressures between 10^{-7} and 10^{-4} Pa for laser pulse energies between 0.1 and 0.3 mJ and then corrected for changes in the laser pulse energy using the measured intensity (pulse energy) dependence of the CO REMPI signals (see Fig. 6 and Sec. IV, below). The corrected data exhibit a linear dependence upon the CO pressure, with scatter about a best fit linear regression of $\pm 10\%$–15%, while the uncorrected data exhibit variations as large as $\pm 40\%$. The deviations from the best fit linear regression are displayed in Fig. 7. It is clear from this figure that there is no additional systematic pressure dependence, beyond the expected linear relation, for the laser pulse energy corrected data. Therefore, once the precise relationships between REMPI signal, laser intensity and pressure have been established, i.e., the system has been calibrated, CO pressure measurements within an uncertainty of 10%–15% are fea-

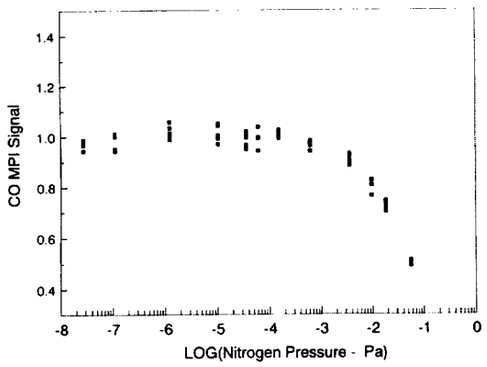

FIG. 8. The dependence of the CO REMPI signal on N_2 pressure at a fixed CO pressure. The loss of CO REMPI signal at high pressure is due to ion scattering in the TOF drift tube at high pressure.

sible. Further improvement is possible by correcting for the laser pulse energy as well as the spatial and temporal fluctuations on a pulse-to-pulse basis.

D. CO REMPI signal dependence on total pressure

Several measurements were performed to determine if there was any dependence of the CO REMPI signal on the total gas pressure. For these measurements we chose to use N_2 as the pressurizing agent, in part because distinguishing between CO and N_2 is a classic mass spectroscopic test. The detection of low pressures of CO in an overwhelming background of N_2 clearly displays the highly selective nature of REMPI in distinguishing between molecular species of same unit mass. For the total pressures used in these experiments ($<10^{-2}$ Pa) the effects of intermolecular collisions (i.e., quenching) would not be expected to be important as the collision rate at 10^{-2} Pa ($\sim 10^4$ s^{-1}) is still several orders of magnitude smaller than the radiative decay rate ($\sim 10^7$ s^{-1}). It would be expected that at the highest pressures ion scattering in the TOF drift tube may cause a loss in total ion signal. We first established a CO pressure of 2×10^{-6}Pa using one of the ballast tank/leak valve inlet systems and verified that the CO REMPI signal level was stable. Then all of the hot filaments [i.e., BA gages and quadrupole mass spectrometer (MS)] were abruptly switched off. Upon switching the ion gages off, it was found that the CO REMPI signal initially dropped by a large factor, as much as 2. The initial drop in CO levels is presumably due to the pumping action of the newly created cold surfaces. After about 30–45 min, the CO REMPI signals had returned to within several percent of the signal levels established prior to switching off the hot filaments. Then, using the second ballast tank and leak valve inlet system, N_2 was introduced into the chamber and the CO REMPI signals were monitored as a function of the N_2 pressure. Here N_2 pressures were determined using the spinning rotor gage located on the high pressure side of the leaky valve and the measured pressure ratio across this valve. The results for one such set of measurements are displayed in Fig. 8. We found that the CO REMPI signal levels did not change as a function of N_2 pressure for pressures less than 10^{-3} Pa, and that there is a definite loss in CO ion collection efficiency at pressures above 10^{-3} Pa, presumably due to ion–molecule scattering in the TOF drift tube. We note also that the observed CO REMPI signals were not independent of N_2 pressure for measurements performed when the hot cathode ionization gages were on. The reason for the N_2 pressure dependence of the CO REMPI signals in the presence of hot cathodes is not fully understood. One possibility is CO generation at the surface of the hot tungsten surface from O_2, CO_2, or H_2O impurities in the N_2 gas stream. This is the subject of further study.

E. Photon stimulated desorption background

Upon introducing the UV laser beam into the vacuum chamber, there is a discernable rise in the background pressure as indicated by the ionization gages and a noticeable change in the residual gas spectrum on the quadrupole mass spectrometer. The measured change in total pressure in the chamber is on the order of $5–7\times10^{-9}$ Pa. The residual gas spectrum recorded by the quadrupole exhibits a rise in the CO and CO_2 signal levels of a factor of about 2, presumably due to photon stimulated gas desorption from the vacuum chamber walls. Photon stimulated desorption from the vessel walls then will limit the ultimate pressure measurement one can make. One curious feature in the residual gas spectrum displayed by the quadrupole mass spectrometer was an observed and quite repeatable change in the residual gas cracking pattern. In the presence of the UV laser beam, the C^+ and O^+ daughter peaks are each about an order of magnitude larger than without UV beam present.

F. Ultimate CO pressure measurements using REMPI-TOF

At base vacuum, without the deliberate introduction of CO into the vacuum chamber, there is still a small CO residual pressure. A certain amount of CO is evolved from the hot cathode gages and is thought to arise from thermal desorption from the gage structure. We used the calibrated CO REMPI technique to measure the amount of CO present in the system at base vacuum as a function of the number of hot filaments present in the vacuum chamber, and the results of these measurements are plotted in Fig. 9. With all three hot cathode ionization gages on the CO pressure measured in the chamber using REMPI-TOF was 8×10^{-8} Pa. Upon turning off one of the BA ionization gages, the CO level dropped to 4×10^{-8} Pa. Upon turning the other BA gage off, the CO pressure dropped further to 2×10^{-8} Pa, and after turning off the quadrupole mass spectrometer so that no hot filaments were operating, the CO pressure stabilized to 4×10^{-9} Pa, a value which is very close to the measured change in chamber pressure due to photon stimulated desorption. At these very low CO pressures the number of laser shots needed to maintain a reasonable signal to noise ratio ($S/N>7$) had to be increased from 500 laser shot averages to 1000. At these

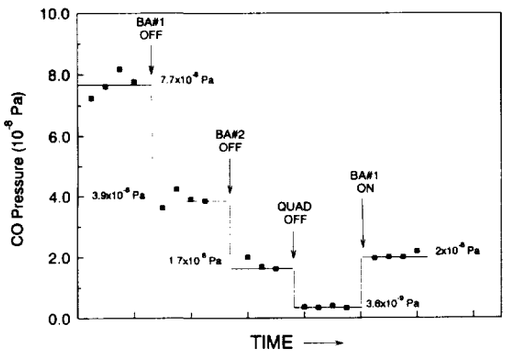

FIG. 9. CO pressure at base vacuum measured by CO REMPI as a function of the number of hot filaments operating. The abrupt changes in the CO signal levels occur when a hot filament is turned off or on, as indicated.

pressures a better measurement scheme would involve the use of ion counting methods for quantification of the ion signals. Also, in order to measure pressures below this level in our system, specific measures would need to be taken to reduce the amount of scattered UV radiation present in the chamber (e.g., by use of Brewster windows).

Upon turning the first of the BA gages back on, an initial pressure rise of about 2×10^{-8} Pa was noted. This pressure rise was about a factor of 2 smaller than what was observed when the gage was turned off, a result which is somewhat surprising. This apparent discrepancy is thought to arise from the fact the entire gage structure was not yet in thermal equilibrium and was still heating up when the laser measurements were terminated. This is a point which warrants further study.

With the present measurement system and 5000 laser shot averages (about 8 min measurement time), the ultimate detection limit would be about $2\text{–}5\times10^{-10}$ Pa for a $S/N>2$. Using the theoretical model for the REMPI signal developed in Sec. IV, we estimate that about one in 10^5 of the molecules within the collection volume is ionized per laser pulse for a laser intensity of 10^9 W/cm^2. For these conditions a single ion would be created per laser pulse at a pressure of about 10^{-10} Pa.

IV. DISCUSSION

As fluctuations and drifts in the laser pulse energy (and hence intensity) are unavoidable when using pulsed laser systems and frequency doubling schemes for UV light generation, compensation for systematic changes in laser intensities is necessary if quantitative pressure measurements are to be achieved. To this end, we develop a semiempirical model for the ion yield per laser pulse which is used to normalize the measured signals. Through the development of this model we will also gain further insight into the ionization process and its dependence on laser parameters.

For a single laser pulse the number of ions detected is given by

$$N_{\text{ions}}=fN^+, \tag{1}$$

where f is the detection efficiency of the TOF-MS system and N^+ is the number of ions created by the laser pulse. N^+ is, in turn, given by

$$N^+=\int\int\int_v\left(\int_\tau \dot{n}^+(I)dt\right)dx\,dy\,dz \tag{2}$$

$$=\int\int\int_v n^+(I)dx\,dy\,dz, \tag{3}$$

where

$$n^+(I)=\int_\tau \dot{n}^+(I)dt \tag{4}$$

and $\dot{n}^+(I)$ is the number density of ions created per unit time in the ion collection region of the TOF-MS and I is the laser intensity. Here the integrations extend over the entire ion collection volume and over the temporal evolution of the laser pulse. The spatial dependence of the number density of ions created arises from the spatial and temporal variations of the laser intensity over the ion collection region of the TOF-MS, that is

$$\dot{n}^+(I)=\dot{n}^+[I(x,y,z,t)]. \tag{5}$$

An expression for $n^+[I(x,y,z)]$, the number of ions per unit volume created as a function of position, in terms of the number density of CO molecules is derived from rate equation analysis with the following simplifying observations. For linearly polarized light the dependence of the transition moment of the two-photon transitions strongly favors excitation of the Q branch by at least $100\times$ over S or O branch excitation,[15] indicating negligible cross J population in the two-photon excitation step. Next, we note that the observed spectrum is very well modeled by two-photon absorption theory[15] and also note that the photoionization from the $B\,^1\Sigma^+(v=0)$ state at 345 nm has been shown to be J independent,[13] indicating that the ionization is J independent at least over a limited wavelength region. This allows us to simplify the problem to that of a three-level system. At the pressures used in these measurements (below 10^{-4} Pa), the mean free path of the CO molecules is several tens of meters and hence collisional quenching of the $B\,^1\Sigma^+(v=0)$ state is unimportant. For the low rotational levels of the $B\,^1\Sigma^+(v=0)$ state, CO exhibits no predissociation,[16] and we conclude that the primary loss mechanism of the $B\,^1\Sigma^+(v=0)$ state in these experiments is radiative decay. With these assumptions, the rate equations relevant to our experimental conditions can be written (see Fig. 1)

$$\frac{dn_0}{dt}=-\frac{\alpha I^2}{h\nu}(n_0-n^*), \tag{6}$$

$$\frac{dn^*}{dt}=\left(\frac{\alpha I^2}{h\nu}\right)(n_0-n^*)-\left(\frac{\sigma I}{h\nu}+A\right)n^*, \tag{7}$$

$$\frac{dn^+}{dt}=\left(\frac{\sigma I}{h\nu}\right)n^*, \tag{8}$$

where n^+, n^*, and n_0 are the respective number densities of ion, excited electronic and ground state CO molecules, α is

the two-photon absorption cross section for the $B\,^1\Sigma^+ \leftarrow X\,^1\Sigma^+$ (0,0) transition, σ is the (one photon) ionization cross section for the $B\,^1\Sigma^+(v=0)$ state at 230 nm, A is the radiative decay rate of the $B\,^1\Sigma^+(v=0)$ state and I is the local laser intensity (implicitly a function of position). By approximating the temporal evolution of the laser pulse as a rectangle of intensity I and duration t, we can solve Eqs. (6)–(8) exactly by Laplace transform techniques.[24] The result for the ion density at the end of the laser pulse (time t), with the assumption that all CO molecules are in the ground state before the arrival of the pulse, is

$$n^+(x,y,z)=\frac{\beta\lambda N_0}{\theta_+-\theta_-}\left(\frac{(1-e^{-\theta_- t})}{\theta_-}-\frac{(1-e^{-\theta_+ t})}{\theta_+}\right) \quad (9)$$

$$=N_0 S[I(x,y,z)], \quad (10)$$

where N_0 is the number density of CO molecules, β is the rate of ionization ($=\sigma I/h\nu$), λ is the two-photon absorption rate ($=\alpha I^2/h\nu$). $\theta_{+,-}$ are given by

$$\theta_{+,-}=\tfrac{1}{2}[(A+\beta+2\lambda)\pm\sqrt{(A+\beta+2\lambda)^2-4\lambda(A+\beta)}]. \quad (11)$$

To model the intensity dependence of the CO REMPI signal, four quantities are now needed; the spatial variation of the laser beam over the collection volume, the two-photon $B\,^1\Sigma^+ \leftarrow X\,^1\Sigma^+$ (0,0) absorption cross section (α), the 230 nm ionization cross section for the $B\,^1\Sigma^+(v=0)$ state (σ) and the radiative decay rate ($A=1/\tau$) where τ=radiative lifetime).

The radiative lifetime of the $B\,^1\Sigma^+(v=0)$ state has been studied by a number of researchers using a number of different techniques[17] and has been determined to be 25 ± 4 ns, which corresponds to a deexcitation rate of $4.0\pm0.5\times10^7$ s^{-1}. The spatial distribution of the laser intensity was measured by using a CCD camera. We assume that the recorded CCD camera images are representative of the laser intensity distribution over the course of the measurements. The CCD camera provides the *relative* spatial distribution of intensities in the x–y plane, $g(x,y)$, and by using the measured pulse energy P_e and the pulse duration t, the intensities are calculated using

$$I(x,y)=\left(\frac{P_e}{aht}\right)g(x,y), \quad (12)$$

where a is the total area of the image which contributes to the total intensity and h is the average image "height" over the area a. This gives the correct normalization so that the integral of $I(x,y)$ over the entire image yields P_e/t, the total power in the laser pulse.

This now reduces the number of unknowns in Eq. (9) to only two: the ionization cross section and the two-photon absorption cross section. We have found two reports of two-photon absorption cross section measurements in the literature. One study by Tiee *et al.*[25] found $\alpha\approx1\times10^{-30}$ cm^4/W, while Bergstrom *et al.*[18] report a value some three orders of magnitude larger, $\alpha\approx10^{-27}$ cm^4/W. The 230 nm single-photon ionization cross section has not been measured directly. For the ionization cross section Bergstrom *et al.*[18] report $\sigma=2\times10^{-17}$ cm^2 at 355 nm for the $B\,^1\Sigma^+(v=0)$ state, while Ferrel *et al.*[26] found $\sigma=1.4\times10^{-19}$ cm^2 for the $B\,^1\Sigma^+(v=0)$ level at 302 nm. By fitting Eq. (9) to our REMPI signal versus P_e, we determine an effective value for the ionization cross section, $\sigma_{\text{eff}}=7\times10^{-18}$ cm^2, which is in reasonable agreement with the value of Bergstrom *et al.*[18] The result of this calculation is indicated by the solid line on Fig. 6. Here we have also used a value for the two-photon cross section of $\alpha=10^{-27}$ cm^4/W. However, the exact value of the two-photon cross section is immaterial as the REMPI signal versus pulse energy curve will only place an upper bound on the value of α. The difference in the value of our ionization cross section and that reported by Bergstrom *et al.*[18] could quite possibly be attributable to the use of the rectangular pulse approximation in the derivation of Eq. (9) instead of a more realistic laser pulse shape. Given the level of agreement between our value and Bergstrom's, it would appear that the rectangular pulse approximation is reasonable for this level of precision.

Finally, by combining Eqs. (1), (3), and (10), we can write the relation between the CO number density N_0 and the measured ion signal in the form

$$N_0=\frac{\xi N_{\text{ions}}}{fL\int\int_\sigma S[I(x,y)]\,dx\,dy}, \quad (13)$$

where L is the spatial extent of the ion collection region along the laser propagation direction (=3 mm), the x–y integration extends over the laser intensity profile in the focal plane and ξ is a suitable scale factor. Equation (13) is used to correct the measured ion signals ($=\xi N_{\text{ions}}/f$) for variations in the laser intensity and/or pulse energy.

Although the approach to the measurement of other gases will be similar to that discussed here, the details of the dependence of the ion signals on laser intensity and the wavelength dependence of the observed REMPI spectrum will be quite different. Almost any gas species can detected using REMPI and quantitative pressure measurements in the UHV regime using REMPI-TOF are certainly feasible for a number of other species of interest, including O_2, CO_2, NO, and, perhaps, H_2O. However, there may be practical limitations to the application of REMPI to some gas species, and the ionization of CO through the $B\,^1\Sigma^+$ state represents, in many ways, an ideal molecular case. The Franck–Condon factor for the $B\,^1\Sigma^+ \leftarrow X\,^1\Sigma^+$ (0,0) transitions is nearly unity, and the difference in the rotational constants for the ground and excited electronic states is small, thus the $B\,^1\Sigma^+ \leftarrow X\,^1\Sigma^+$ (0,0) transitions exhibit a compact Q-branch head. In applying REMPI to other molecules, electronic transitions with Franck–Condon factors less than unity and larger differences in the rovibrational structures of the ground and excited electronic states will be expected, and transitions will not, in general, exhibit such compact branch heads. Overall then, lower ionization efficiencies would be expected for other molecules or other transitions within the CO molecule. Also, the ionization cross section of the $B\,^1\Sigma^+$ state is large enough so that for moderate laser intensities nearly complete saturation of the ionization step is possible which

helps to reduce the dependence of the ion signal on laser power fluctuations. We have briefly investigated REMPI detection of O_2 and N_2 and have found it quite possible to detect these species in the UHV regime using either 2 or 3 photon resonant, 3 or 4 photon ionization near 288 nm. The signal strengths found were about 2 orders of magnitude smaller than the corresponding CO signals, indicating that the ultimate partial pressure detection limits for these species may not be as low as that found for CO. Furthermore, 3+1 ionization of N_2 should also display an I^4–I^3 ion signal dependence, and hence the scatter in the data associated with pulse energy, spatial and temporal fluctuations of the laser beam would then be amplified above the 10%–15% level found in the CO measurements. Therefore, while the extension of the ideas presented here to other species is straightforward, the practical implementation will require additional work.

V. CONCLUSIONS

The data in Fig. 7 indicate that the CO ion signal measured is linear with CO number density over the pressure range 10^{-7}–10^{-4} Pa and that measurements with uncertainties of ±10%–15%, or better, are possible when variations for fluctuations in the laser pulse energy are accounted for properly. We have also found that CO measurements down to 10^{-10} Pa are possible, even in an overwhelming N_2 background. While REMPI-TOF measurements may not find the widespread application of conventional vacuum measurements, this technique does allow for the quantitative, species specific measurement of active gases without the perturbations attendant on the operation of conventional vacuum instrumentation. Therefore, REMPI-TOF represents a promising research tool for accessing measurement errors and other effects associated with active gas-instrument interactions and the measurement of fundamental physical phenomena at low pressures.

ACKNOWLEDGMENTS

The authors would like to thank C. R. Tilford for several helpful discussions, A. S. Pine for the use of the Nd:YAG laser, D. F. Martin for his expert technical assistance in the construction of the TOF-MS, and P. J. H. Tjossem for the CO two-photon absorption simulation program. This work was sponsored in part by The Primary Standards Laboratory of Sandia National Laboratories.

[1] J. H. Singleton, J. Chem. Phys. **45**, 2819 (1966).
[2] J. A. Becker, E. J. Becker, and R. G. Brandes, J. Appl. Phys. **32**, 411 (1961).
[3] P. A. Redhead, Vacuum **13**, 253 (1963).
[4] H. Zacharias, H. Rottke, and K. H. Welge, Appl. Phys. **24**, 23 (1981); H. Zacharias, R. Schmiedl, and K. H. Welge, *ibid.* **21**, 127 (1980).
[5] R. L. Chien and M. R. Sogard, J. Vac. Sci. Technol. A **8**, 2814 (1990).
[6] K. Kokoburn *et al.*, J. Vac. Sci. Technol. A **8**, 3310 (1990).
[7] J. D. Fassett, L. J. Moore, J. C. Travis, and J. R. DeVoe, Science **230**, 262 (1985).
[8] J. D. Fassett and J. C. Travis, Spectrochim Acta B **43**, 1409 (1988).
[9] C. H. Chen *et al.*, in *Lasers and Mass Spectroscopy*, edited by D. Lubman (Oxford, London, 1990), pp. 3–36.
[10] W. G. Mallard, J. H. Miller, and K. C. Smyth, J. Chem. Phys. **76**, 3483 (1982).
[11] T. A. Cool, in Ref. 9, pp. 446–467.
[12] P. J. H. Tjossem and K. C. Smyth, Chem. Phys. Lett. **144**, 51 (1988).
[13] H. Rottke and H. Zacharias, Opt. Commun. **55**, 87 (1985).
[14] T. A. Cool, Appl. Opt. **23**, 1559 (1984).
[15] P. J. H. Tjossem and K. C. Smyth, J. Chem. Phys. **91**, 2041 (1989).
[16] D. Coster and F. Brons, Physica **1**, 155, 634 (1934), D. N. Read, Phys. Rev. **46**, 571 (1934).
[17] See T. A. Carlson, N. Duric, P. Erman, and M. Larsson, Z. Phys. A **287**, 123 (1978), and references therein.
[18] H. Bergstrom, H. Lundberg, and A. Persson, Z. Phys. D **21**, 323 (1991).
[19] D. A. Dahl and J. E. Delmore, computer code SIMION (Idaho National Engineering Laboratory, Idaho Falls, ID, 1988).
[20] J. K. Fremerey, J. Vac. Sci. Technol. A **3**, 1715 (1985).
[21] S. Dittmann, B. E. Lindenau, and C. R. Tilford, J. Vac. Sci. Technol. A **7**, 3356 (1989).
[22] L. Lieszkovszky, A. R. Filippelli, and C. R. Tilford, J. Vac. Sci. Technol. A **8**, 3838 (1990).
[23] T. S. Eichelberger IV and G. J. Fisanick, J. Chem. Phys. **74**, 5962 (1981).
[24] G. Arfken, *Mathematical Methods for Physicists*, 3rd ed. (Academic, New York, 1985).
[25] J. J. Tiee, C. R. Quick, Jr., G. W. Loge, and F. B. Wampler, J. Appl. Phys. **63**, 288 (1988).
[26] W. R. Ferrell, C. H. Chen, M. G. Payne, and R. D. Willis, Chem. Phys. Lett. **97**, 460 (1983).